Lidar observations of the Planetary Boundary Layer above the city of Thessaloniki, Greece

V. Santacesaria [1](*), F. Marenco [1](**), D. Balis [1]
A. Papayannis [1][2] and C. Zerefos [1]

[1] *Aristotle University of Thessaloniki, Laboratory of Atmospheric Physics*
   Campus Box 149, 54006 Thessaloniki, Greece
[2] *National Technical University of Athens, Laser and Applications Laboratory*
   Zografou Campus, Heroon Polytechniou 9, 15780 Zografou, Greece

Summary. — Aerosol measurements have been performed in Greece since 1994, using a backscattering lidar system. The main scientific objective has been to evaluate the vertical structure of the Planetary Boundary Layer (PBL) in urban sites of Greece, using suspended aerosols as tracers of the atmospheric motion. The observations presented here were performed in early 1996, over the city of Thessaloniki in Northern Greece, close to the sea shore. The lidar system was operated under varying air pollution and meteorological conditions. The vertical profiles of the aerosol extinction and backscattering coefficients were retrieved from the lidar signal, using the Fernald-Klett inversion algorithm. Comparison between standard meteorological data from radiosondes and ground stations proves that lidar aerosol profiles can be successfully used to monitor the time variation in the layering of the lower troposphere.

PACS 96.20 – Meteorology.

1. – Introduction

The PBL is the lowest part of the atmosphere: it is directly influenced by the presence of the Earth's surface, and responds to surface forcing with a time scale of about an hour or less [1]. Surface forcing includes frictional drag, evaporation and

---

transpiration, heat transfer, pollutant emission and terrain-induced flow modification. The Boundary Layer thickness is variable in time and space, ranging typically from a few hundred meters up to 1-2.5 km. Its depth depends on the nature of the surface (land or ocean) and on the meteorological conditions. Over the sea the depth of the PBL is almost uniform in space and in time. Its variability is within 10% in a range of 1000 km. Changes are essentially due to the synoptic process of vertical motion or advection of air masses. On the other hand, over the land, the PBL structure shows a great variability which is strongly correlated to the solar zenith angle and to the orography of the area of interest.

Both for the land and the ocean, the PBL is thinner in a high-pressure field than in the case of low pressures. In strong meteorological perturbations, it is difficult to define the limit of the PBL, and in those cases there is no distinction between the PBL and the free troposphere.

Internal sublayers of the PBL are often identified, namely:

– Mixed layer (or convective boundary layer): characterised by highly developed vertical motion and convection. The turbulence is essentially associated with heat transfer from the ground, being heated up by sunlight during daytime, to the higher layers, characterised by radiative cooling. During stable metereological conditions, the depth of the mixed layer depends mainly upon the diurnal cycle of ground temperatures: it is formed at sunrise, and its maximum depth is usually found in the late afternoon, when it can take the extension of the whole PBL. The potential temperature profile of the mixed layer is superadiabatic near the ground, and almost adiabatic in the upper part.

– Entrainment zone: characterised by a dynamically stable atmosphere (temperature inversion). The potential temperature profile is subadiabatic. This layer acts as a lid to the rising thermals. It is found at the upper limit of the mixed layer.

– Stable boundary layer: it replaces the mixed layer and entrainment zone when the potential temperature profile is subadiabatic, and thus the air mass is stable.

– Residual layer: this is the name given to the mixed layer, when the degree of turbulence decays due to reduced surface heating. Usually, this happens close to sunset. The potential temperature profile is nearly adiabatic.

The criteria used to identify the layers are described in detail in the literature [1]. The above-mentioned layers, usually, are not present at the same moment. For instance, the mixed layer and the entrainment zone are mostly present during the day, and turn into the residual layer after sunset; a stable boundary layer appears later on. The latter can then be transformed into a new entrainment zone on the next morning, after sunrise, if the day is clear: the mixed layer appears below it, and pushes it up. During the transition from night to day (and viceversa), copresences of the layers are possible. The PBL evolution does not have to strictly follow this "typical" pattern, proper of clear summer days and high-pressure fields. It is important to note that different meteorological conditions result in different patterns of the PBL structure, which thus presents a high variability from day to day.

Since the source of many aerosols is on the Earth's surface, the PBL often contains high concentrations of aerosols. The concentration, chemical composition and particle size distribution of the atmospheric aerosols are highly variable, in both time and space. As a consequence, the aerosol optical properties present a large spatio-temporal variation.

Lidar systems are gaining high acceptance as long-range, non-invasive spectro-scopic probes of the chemical composition and properties of the atmosphere [2-6]. Lidar techniques have been developed to study the structure of the atmosphere, by means of the elastic and non-elastic scattering of laser light from atmospheric gases and suspended particulates (aerosol). By using the aerosols as tracers of the atmospheric dynamics, the lidar is a powerful tool for visualizing, in real time, several parameters of the PBL structure with high temporal and spatial resolution. Therefore, a backscattering lidar can provide information on the PBL structure, mixed-layer depth, entrainment zones and convective cells structure, aerosol distribution, clear air layering, condensation levels, cloud-top altitudes, cloud statistics, atmospheric transport, low-level jets, diffusion processes, and other inferences of air motion [1, 7-11].

The backscattered energy is approximately proportional to the aerosol content of the observed air mass. However, several assumptions would have to be made regarding the unknown parameters (particle size, shape, refractive index), if absolute mass density or number density measurements were required.

The purpose of this paper is to describe the performance of the mobile backscattering lidar at the Laboratory of Atmospheric Physics (LAP) in studying the diurnal variations in the spatial properties of the PBL (PBL height and internal structure). Section **2** explains, briefly, the experimental set-up, while sect. **3** presents the lidar data inversion algorithm used in this paper. Section **4** contains correlations of standard meteorological data measured by radiosondes to similar occurrences observed by the lidar system. Lastly, sect. **5** presents a discussion and our concluding remarks.

2. – Experimental set-up

The lidar in the Laboratory of Atmospheric Physics (LAP) of the Aristotle University of Thessaloniki is a mobile system, and has been described in detail by Papayannis *et al.* [12]. In early 1996, it was operated at an altitude of 60 m above sea level from the roof of the Physics building in the Thessaloniki University campus (41°N, 23°E). The emitter beam is coaxial to the receiver field of view, it points vertically to the zenith. It is based on a Nd:YAG pulsed laser with second- and third-harmonic generators, operated at 10 Hz prf. The pulse energy is 650 mJ at 1064 nm, 110 mJ at 532 nm, and 80 mJ at 355 nm. However, only the last two wavelengths are used at present. The lidar receiver includes a 30.5 cm Newtonian telescope (1.5 m focal length), a harmonic separator beam splitter, two narrow-band interference filters (1 nm FWHM at 355 nm and 0.1 nm FWHM at 532 nm), and two photomultiplier tubes (PMT).

A complete overlap between the laser beam and the telescope field of view is expected at a range of 600 m, as has been estimated by geometrical form factor calculations performed according to Halldorsson and Langerholc [13]. This value represents the lower limit of our vertical lidar profiles. The signal acquisition is done in the analog mode by a 1 GS/s digitizing oscilloscope, which acts both as an analog-to-digital converter and as a waveform recorder. A personal computer (PC) equipped with a GPIB interface PC card (IEEE 488.2) drives the oscilloscope, averages the lidar profiles over time, and stores the lidar data on the PC hard disk. The vertical and temporal resolutions of the lidar system were set to 15 m and 10 min, respectively.

3. – Lidar inversion algorithm

The inversion of the lidar profiles is based on the solution of the classical lidar equation for the case of single scattering [14]:

$$(1) \qquad P(\lambda, R) = P_{\mathrm{L}} A_0 \, \frac{\xi(\lambda)}{R^2} \, \beta(\lambda, R) \, \varsigma(R) \, \frac{c\tau_1}{2} \, \exp\left[-2 \int_0^R \alpha(\lambda, R) \, \mathrm{d}R \right],$$

where $P(\lambda, R)$ is the lidar signal received from a distance R at wavelength λ, P_{L} is the emitted laser power, A_0 is the telescope-receiving area, $\xi(\lambda)$ is the receiver's spectral transmission factor, $\beta(\lambda, R)$ is the atmospheric volume backscattering coefficient, $\varsigma(R)$ is the overlap factor between the field of view of the telescope and the laser beam, $\alpha(R)$ is the attenuation coefficient from atmospheric molecules, c is the light speed and τ_1 is the laser pulse length.

The lidar data have been processed with the algorithm described by Fernald [15] and Klett [16], and assuming to know the molecular (or Rayleigh) contribution to the signal from the US Standard Atmosphere [17]. According to the Fernald-Klett formulation, the solution of the lidar equation is given by the following formula:

$$(2) \qquad \beta(R) = \frac{\exp\left[-(S'(R_{\mathrm{ref}}) - S'(R)) \right]}{1 \Big/ \beta(R_{\mathrm{ref}}) + \dfrac{2}{C} \displaystyle\int_R^{R_{\mathrm{ref}}} \mathrm{d}R' \, \exp\left[-(S'(R_{\mathrm{ref}}) - S'(R')) \right]},$$

where $\beta(R) = \beta_{\mathrm{p}}(R) + \beta_{\mathrm{R}}(R)$ (particulate and Rayleigh contribution), $\beta(R_{\mathrm{ref}})$ the boundary condition set on $\beta(R)$ at the reference far-end range R_{ref};

$$(3) \quad S'(R_{\mathrm{ref}}) - S'(R) =$$

$$= \ln\left[R_{\mathrm{ref}}^2 * P(R_{\mathrm{ref}}) \right] - \ln\left[R^2 * P(R) \right] - \frac{3}{4\pi} \int_R^{R_{\mathrm{ref}}} \beta_{\mathrm{R}}(R') \, \mathrm{d}R' + 2 \int_R^{R_{\mathrm{ref}}} \frac{\beta_{\mathrm{R}}(R') \, \mathrm{d}R'}{C} \ .$$

In this formula, $P(R)$ is corrected for background noise.

To derive the above equation, several assumptions were made: a) the back-scatter-to-extinction ratio ($\beta/\alpha = C$) is known, b) the reference range R_{ref} is taken in a region where the lidar profile followed the molecular atmosphere (generally between 4 and 6 km). The value of $\beta(R)$ at the reference range was accordingly chosen as been equal to $\beta_{\mathrm{m}}(R)$ (no aerosol contribution). The value of C was chosen as been equal to 0.035, which is an average value among those suggested for rural, urban and maritime aerosols [18]. It must be stressed that, due to the position of our experimental site (urban maritime site), it was not possible to easily choose a single aerosol model.

A second approach adopted in this paper, for analysising the results in terms of the dynamics only, consists in the calculation of the vertical gradient $D(R)$ of the lidar

signal [7], expressed as

$$(4) \qquad D(R) = dS(R)/dR = \frac{d(\ln [P(R) \, R^2)}{dR} \; .$$

This method provides a mathematical representation of the boundaries between air masses identified by difference in the aerosol content. Positive gradients of $S(R)$ correspond to increasing backscatter with altitude, and viceversa. A strong decrease with altitude in the aerosol concentration is expected at the entrainment zone, when the emission source is on the ground: this decrease is detectable even without inverting the backscattered echoes to profiles of backscattering and extinction coeefficients [7]. The largest negative vertical gradient in the lidar signal, associated with a sharp transition from "dirty" to "clean" air, can be used to mark this layer.

4. – Selected results

In this section, two cases of correlation between lidar and radiosonde data are presented, as well as the aerosol backscattering coefficients observed during two days of nearly continuous operations. For the purposes of determining the boundaries of the aerosol layers and the vertical structure of the atmosphere, both lidar channels (532 nm and 355 nm) contain equivalent information. Therefore, in each of our plots only one of the channels is shown.

Different meteorological conditions resulted in different patterns of the PBL structure. In the cases presented here, the PBL altitude was found to be within the 1–3 km range, and the corresponding aerosol loads showed a very high variability, on a diurnal time scale and also over a shorter time period.
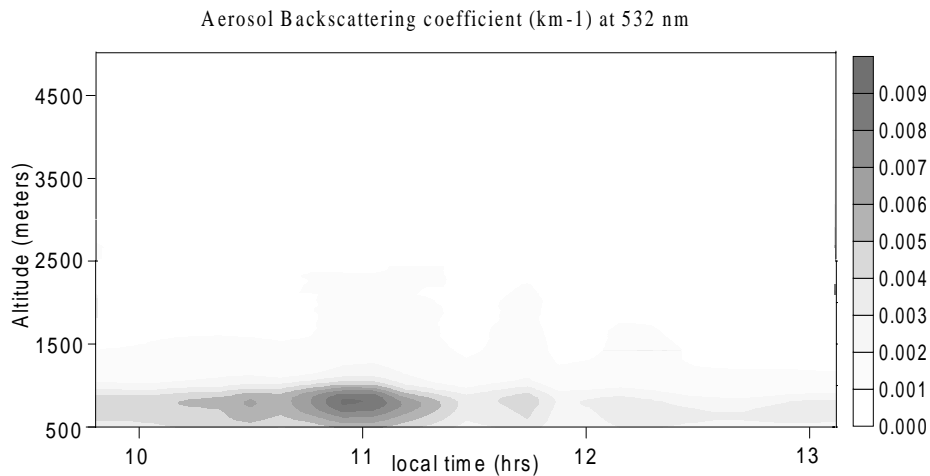

Aerosol Backscattering coefficient (km-1) at 532 nm

Fig. 1. – Time evolution of the aerosol backscattering coefficient (at 532 nm) from 10:00 to 13:00 local time on 17th February 1996. A strong increase of the aerosol backscatter around 11:00 is evident. This perturbation lasted for only half an hour.
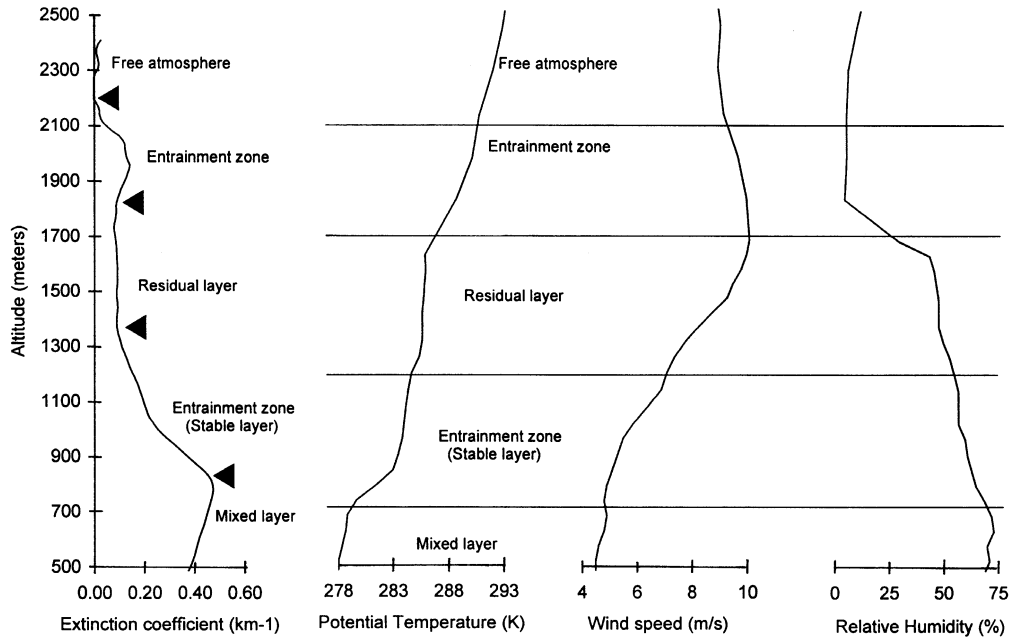
Fig. 2. – Comparison between the extinction aerosol profile (N 532 nm) with radiosonde profiles (temperature, wind speed and relative humidity) performed at the same hour on 17th February 1996 at 12:00 LT. The structure of the PBL obtained from the different data is also reported in the figure. The triangles indicate the apparent transition from one layer to another in the extinction profile, while the same apparent transitions are indicated by lines in the case of the radiosonde.

In some cases, sudden increases of the aerosol backscattering coefficient were observed, sometimes without significant changes in the PBL structure. A good example is the peak in the aerosol load observed around 11:00 LT on February 17th (fig. 1), when the aerosol load doubled for a period of 30 minutes. The profile of the aerosol extinction coefficient at 12:00 LT is shown in fig. 2, together with the profile of the potential temperature, wind speed and relative humidity obtained by a simultaneous radiosounding performed on site at the Makedonian Airport, a short distance (around 5 km) away from the lidar. The top of the PBL can be identified from the radiosonde, as well as from the lidar profile.

The structure of the PBL retrieved from the radiosonde and lidar profile can be observed in the figure.

From the ground up to 700 m the nearly adiabatic potential temperature profile, together with a subgeostrophic wind speed and a high relative humidity, indicated the presence of the mixed layer. The lidar profiles indicated the top of the mixed layer at 800 m.

Above this layer an entrainment layer was present up to 1200 m for the radiosondes and 1350 m for the lidar. This layer was probably the former stable boundary layer, created during the night and pushed up by the mixed layer. The wind speed in this region is subgeostrophic.
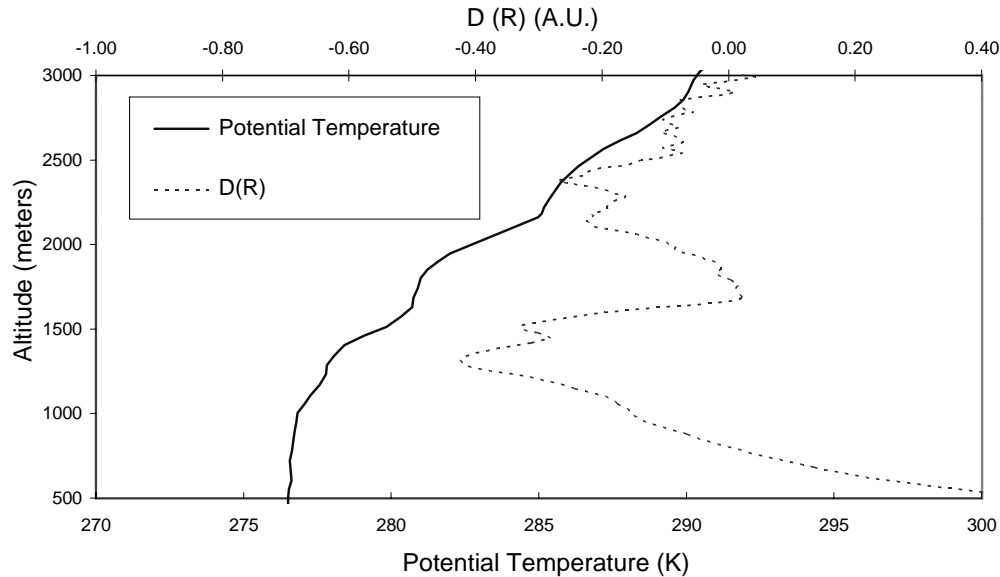
Fig. 3. – Potential temperature profile retrieved from the radiosonde launched at 13:30 on 6 March 1996, plotted together with the lidar signal gradient $D(R)$.

Up to 1700 m a residual layer from the night before was observed in the radiosondes profiles, characterised by a supergeostrophic wind. According to the lidar measurement, the top of the residual layer was around 1800 m.

The top of the PBL and the beginning of the free atmosphere is the altitude at which the aerosol load decreased and where a sharp decrease of relative humidity and a geostrophic wind speed were observed. This was estimated by the radiosondes to be around 2100 m and 2200 m from the lidar measurements.

The small differences can be ascribed to the different locations of the measurements. This discrepancy is comparable to those obtained by Cooper *et al.* [10], in a similar comparison. The wind speed became constant above the PBL, marking the transition to the free troposphere. In this case, the agreement between the information extrapolated from the lidar profiles and those from the radiosonde was acceptable.

In fig. 3, we show simultaneously taken data of the potential temperature profile for March 6th at 13:30 LT together with the signal gradient $D(R)$. The minima of $D(R)$ (strongest aerosol decrease) correspond to temperature inversion layers. The PBL altitude, obtained by the $D(R)$ profile, corresponded to the highest strong minima, that is, 2300 m. The mixed-layer top was located at 1300 m. Using the radiosondes we obtained around 2200 m for the PBL and around 1000 m for the mixing layer. This showed how the quantity $D(R)$ obtained without any inversion of the lidar signal, can yield valuable information on the internal structure of the PBL.

Let us now consider two cases during which the lidar was operated almost continuously for a day. On 1st April, a low-wind regime prevailed, except for a short time between 16:00 and 18:00 (fig. 4). The plot of the lidar data shows that the altitude of the aerosol peak had a maximum in the afternoon; at the same time the surface temperature also reached its maximum. The height of the PBL top, identified as the

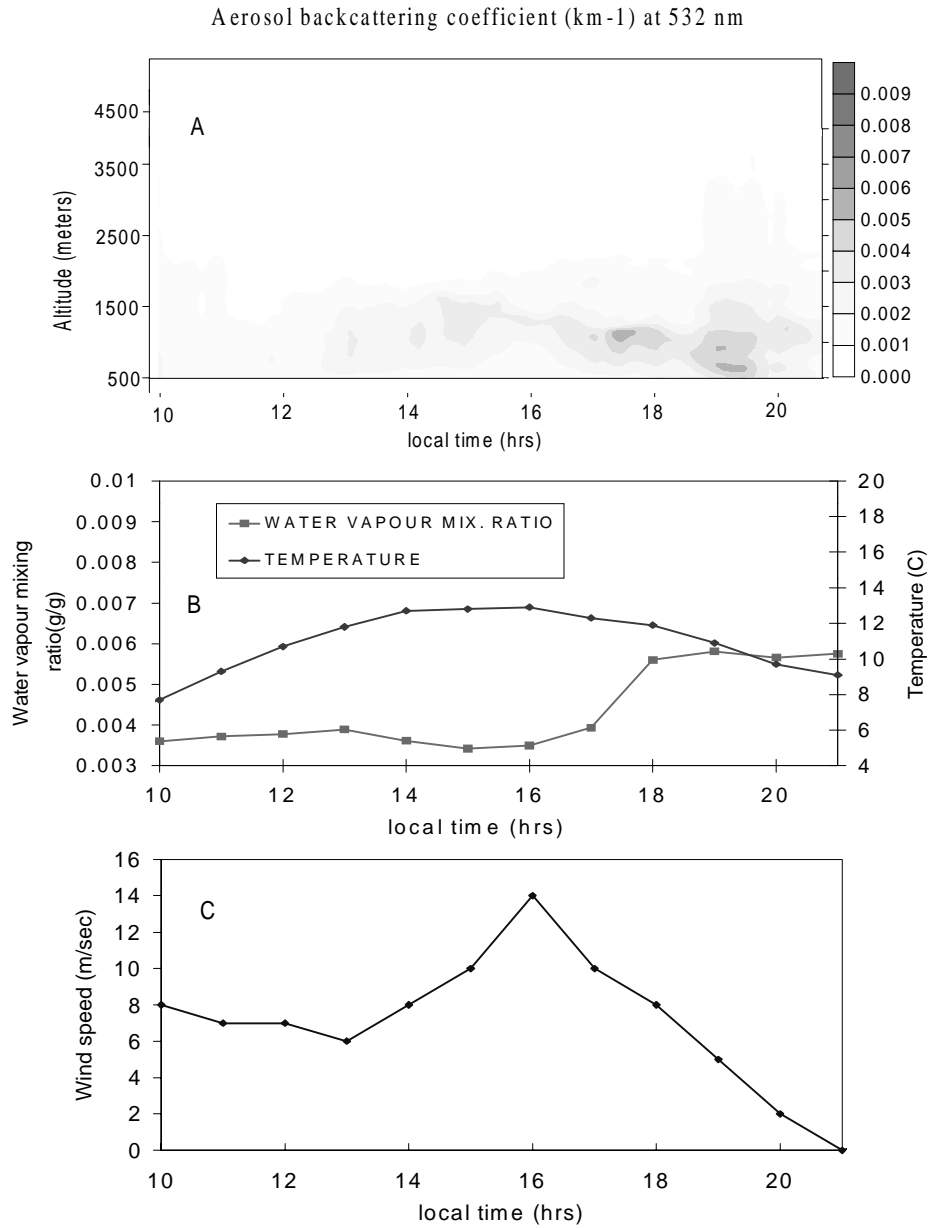Aerosol backcattering coefficient (km-1) at 532 nm

Fig. 4. – Lidar and supplemental data for 1st April 1997. Time evolution of the aerosol backscatter coefficient at 532 nm retrieved by lidar (panel A), of temperature and water vapour mixing ratio at ground level (panel B), and of wind speed (panel C). The data for temperature, water vapour, and wind speed have been recorded at a meteorological station.
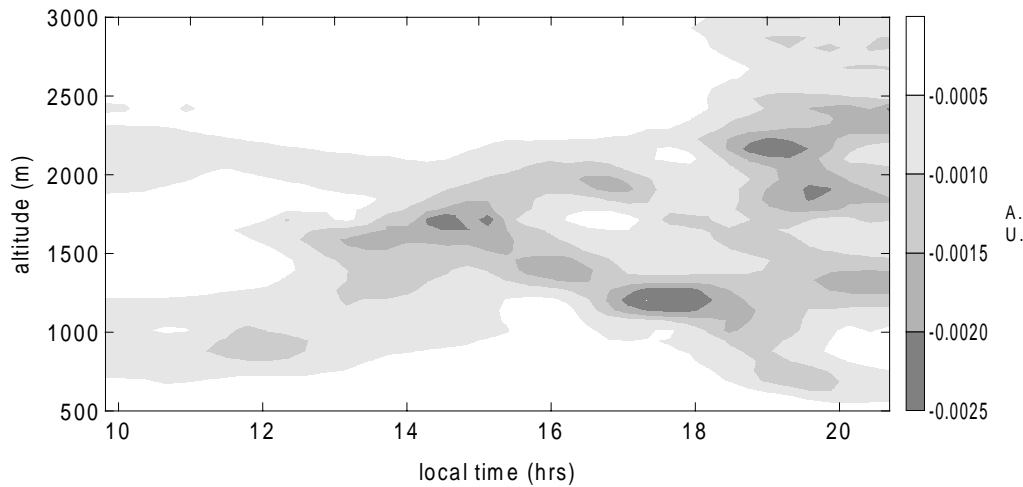
Fig. 5. – Time evolution of the lidar signal gradient $D(R)$ for 1st April 1997. The darker parts correspond to minima of $D(R)$. Around 10:00, two grey bands were present, marking the limit of the mixed layer and PBL, respectively, at 1 km and 2 km. During that day, the PBL height was almost constant. The mixed layer grew until its upper boundary reached the PBL top around 15:00 local time. After 18:00, the plot becomes mostly chaotic (see text).

upper boundary of the aerosol layer, was nearly constant during the day. This "typical" daily evolution of the PBL structure lasted until a little before sunset. To better visualize this evolution, in fig. 5 we present the time-height diagram of $D(R)$. The shaded regions mark the location of the top of the mixed layer and of the PBL, respectively. The depth of the PBL remained more or less constant throughout the day, and the mixed-layer top rose in the morning, reaching the former at about 14:30, and then decreased again, in close relation to the solar zenith angle. After 18:00, a clear increase in the aerosol load was observed (fig. 4). A correlated sharp increase in water vapour mixing ratio at ground level could also be observed, rising from about 0.0035 g/g to about 0.0056 g/g. The increase of the water vapour depended on the change of the wind direction which advected more humid air from the sea after 15:00 LT. The accumulation of the water vapour may have been favoured by the quite strong wind observed between 16:00 LT and 18:00 LT. Later, the mixing ratio stayed almost constant for a few hours. It is probable that the stronger signal aerosol load is correlated to the decrease of the air temperature which could produce an increased condensation of the water vapour on the existing aerosol.

The day 9th April (fig. 6) was characterised by a sea breeze circulation, that strongly affected the structure of the PBL. Moreover, this particular day presented the highest values of aerosol backscatter coefficient. The content of the water vapour of the atmosphere was also very high. The wind reached its maximum intensity at 15:30 LT. At the same time, the aerosol backscattering coefficient and the water vapour mixed ratio reached a minimum. The sea breeze seemed to produce a "clean up" effect on the PBL, resulting in a decrease in the aerosol load and in the humidity. After 18:00 LT, when there was a lower wind speed, we again observed an increase in the aerosol load and in the water vapour mixed ratio over the values in the late morning. Furthermore, the altitude of the aerosol layer (PBL height) was much higher: approximately 3 km.
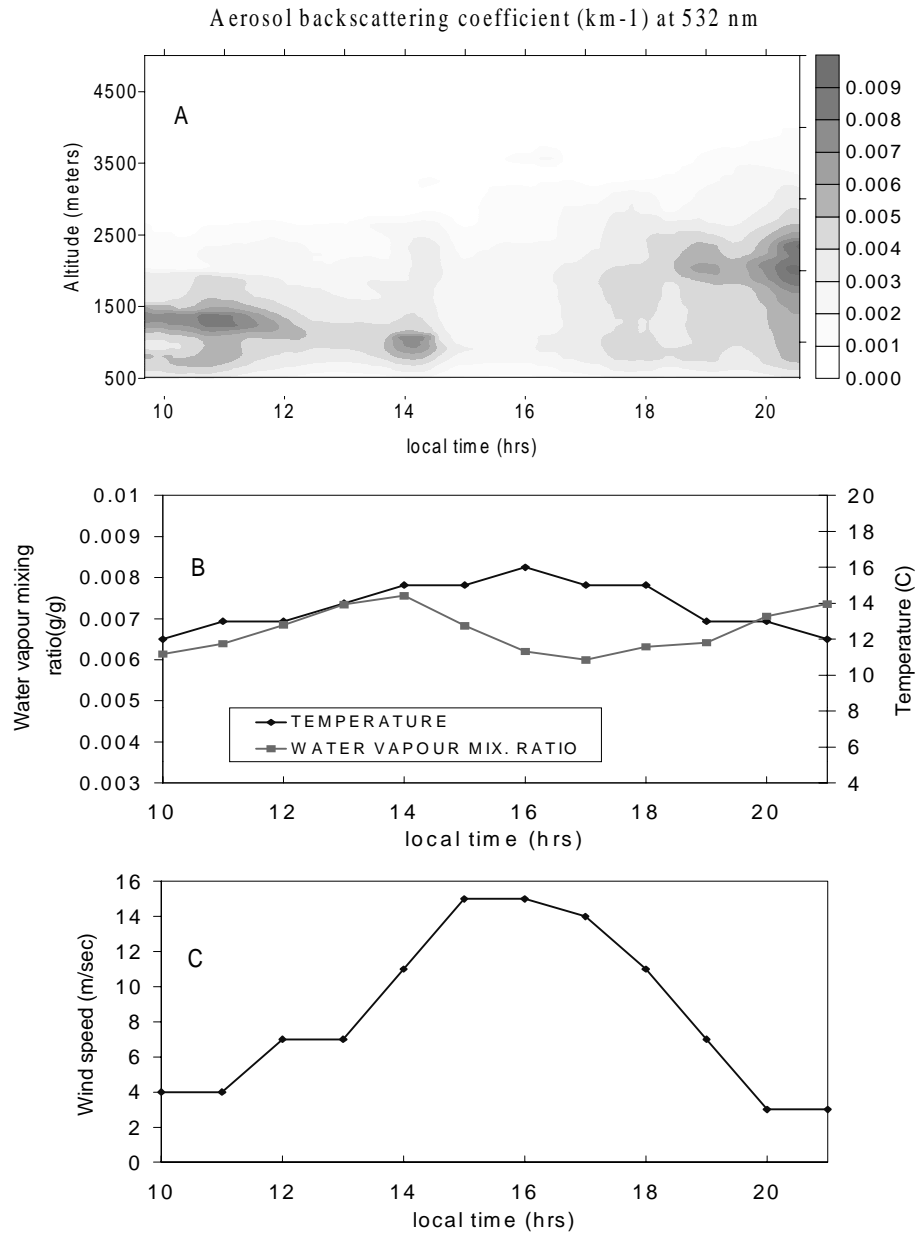
Fig. 6. – Lidar and supplemental data for 9th April 1997. Time evolution of the aerosol backscatter coefficient at 532 nm retrieved by lidar (panel A), of temperature and water vapour mixing ratio at ground level (panel B), and of wind speed (panel C). The data for temperature, water vapour, and wind speed have been recorded at a meteorological station.

5. – Conclusions

With our backscattering lidar we have been able to monitor the structure of the PBL and its diurnal evolution. Different meteorological conditions resulted into different patterns. The altitude of the PBL over the city of Thessaloniki was found to be within the 1.2–3 km range, and the aerosol load showed a very high variability. On 17th February, and 6th March 1996, the structure of the PBL was tested by comparing it with the information obtained by radiosondes launched from the Makedonia Airport. This test was successful.

For 1st and 9th April, more complete lidar aerosol datasets are available. They enhanced two different behaviours of the Thessaloniki PBL. In the first case, characterised by low winds, the mixing-layer depth showed a maximum in the afternoon, correlated with the evolution of surface temperature. In the second case, in the presence of sea breeze, the pattern was that of a PBL with a nearly constant structure. The time at which the wind was strongest was also the time at which both aerosol and water vapour concentrations were lowest, thus showing a "clean-up effect" due to the breeze. In both cases, a strong increase in the aerosol load was seen in the evening, about one hour before sunset, and can possibly be explained in terms of condensation due to surface cooling.

* * *

REFERENCES

[1] STULL R. B., *An Introduction to Boundary Layer Meteorology* (Kluwer Academic Publishers, Dordrecht) 1988.

[2] PELON J. and MEGIE G., *Ozone monitoring in the troposphere and the lower stratosphere: evaluation and operation of a ground-based lidar station, J. Geophys. Res.*, **87** (1982) 4947-4955.

[3] KOLSCH, H., RAIROUX, P., WOLF, J. P. and WOSTE, L., *Simultaneous NO and NO_2 DIAL measurements using BBO crystals, Appl. Opt.*, **28** (1989) 2052-2056.

[4] PAPAYANNIS A., ANCELLET G., PELON J. and MEGIE G., *Multiwavelength LIDAR for ozone measurements in the troposphere and the lower stratosphere, Appl. Opt.*, **29** (1990) 467-476.

[5] ANSMANN A., RIEBESELL M., WANDINGER U., WEITKAMP C., VOSS E., LAHMANN W. and MICHAELIS W., *Combined Raman elastic-backscattered LIDAR for vertical profiling of moisture, aerosol extinction, backscatter and LIDAR ratio, Appl. Phys. B*, **55** (1992) 18-28.

[6] MILTON M., WOODS P. T., JOLLIFFE B., SWANN N. and McILVEEN Mc., *Measurements of Toluene and other Aromatic Hydrocarbons by Differential-absorption LIDAR in the near-ultraviolet, Appl. Phys. B*, **55** (1992) 41-45.

[7] ENDLICH R., LUDWIG E. and UTHE E., *An automatic method for determining the mixed depth from lidar observations, Atmos. Environ.*, **13** (1979) 1051-1056.

[8] MELFI S. H., SPINHIRNE J. D., CHOU S.-H. and PALM S. P., *Lidar observations of vertically organised convection in the Planetary Boundary Layer, J. Clim. Appl. Meteor.*, **24** (1985) 806-821.

[9] CRUM T. D., STULL R. B. and ELORANTA E. W., *Coincident lidar and aircraft observations of entrainment into thermals and mixed layers, J. Clim. Appl. Met.*, **26** (1987) 774-788.

[10] COOPER D. I. and EICHINGER W. E., *Structure of the atmosphere in an urban planetary boundary layer from lidar and radiosonde observations, J. Geophys. Res.*, **99** (1994) 22937-22948.

[11] DEVARA P. C. S., ERNEST RAJ P., SHARMA S. and PANDITHURAI G., *Real-time monitoring of atmospheric aerosols using a computer-controlled lidar, Atmos. Environ.*, **29** (1995) 2205-2215.

[12] PAPAYANNIS A., *The EOLE project: A Greek LIDAR system for ozone and aerosol measurements in the troposphere and the lower stratosphere. Part I: Overview, Int. J. Remote Sensing*, **16** (1995) 3595-3604.

[13] HALLDORSSON T. and LANGERHOLC J., *Geometrical form factors for the LIDAR function, Appl. Opt.*, **17** (1978) 240-244.

[14] MEASURES R., *Laser Remote Sensing of the Atmosphere* (J. Wiley Publ. Co., New York) 1992.

[15] FERNALD F. G., *Analysis of atmospheric LIDAR observations: some comments, Appl. Opt.*, **23** (1984) 652-653.

[16] KLETT J. D., *Lidar inversion with variable backscatter/extinction ratios, Appl. Opt.*, **24** (1985) 1638-1643.

[17] *U. S. Standard Atmosphere, Nat. Ocean. and Atm. Adm., Nat. Aeron. and Space Adm.*, U.S.A.F., Washington D. C. (1976).

[18] KOVALEV V. A., *Lidar measurements of the vertical aerosol extinction profiles with range-dependent backscatter-to-extinction ratios, Appl. Opt.*, **32** (1993) 6053-6065.